High-pressure phases of PbF_2: A joint experimental and theoretical study

H. E. Lorenzana, J. E. Klepeis, M. J. Lipp, W. J. Evans, and H. B. Radousky
Lawrence Livermore National Laboratory, University of California, Livermore, California 94551

M. van Schilfgaarde
SRI International, Menlo Park, California 94025
(Received 23 December 1996)

We report a joint experimental and theoretical study of the dynamical and structural properties of lead fluoride (PbF_2). Specifically, we have performed detailed measurements of the room-temperature Raman-active phonon modes to 310 kbar. We verify the transition at about 4 kbar from the cubic (β) to the orthorhombic (α) phase and the recovery of the α phase at ambient conditions. At approximately 147 kbar, we observe a transformation from the α phase to a modification that we label γ. The data indicate that the γ phase is structurally similar to the orthorhombic α phase. Moreover, we have carried out first-principles calculations which support the existence of a transition in this pressure range, although the crystal structure of the new phase remains undetermined. We have also calculated the equations of state for the two low-pressure phases, β and α. In the case of the α phase, we have made a complete structural determination by calculating the pressure-dependent values of all six internal structural parameters as well as the axial ratios, c/a and b/a, for pressures ranging from zero up to 2 Mbar. Using the calculated α-phase equation of state, we also extract Grüneisen parameters from the data for several optical phonon modes. [S0163-1829(97)04926-6]

I. INTRODUCTION

PbF_2 exhibits remarkably complex and interesting properties despite being one of the simplest ionic solids.[1–5] Recently, PbF_2 has received much attention because of its strong superionic character.[5–7] Studies also indicate that this material has possible applications in high-energy particle detectors.[3,8,9] In particular, the α (orthorhombic) phase can be stabilized at a pressure of a few kbar and recovered at ambient conditions,[5,10] with potentially strong scintillating character.[8,11] Our goal was to investigate the interatomic interactions in PbF_2 at varying particle separations through experiments and calculations. We employed micro-Raman spectroscopy, a powerful technique for remotely and nondestructively evaluating the state of matter at high pressures, to investigate interatomic potentials and crystalline structure through the behavior of phonons. We have also carried out first-principles calculations of the pressure-volume equations of state (EOS) for the α (orthorhombic) and β (cubic) phases, including a determination of the α phase internal structural parameters and their pressure dependence. Using the calculated α phase pressure-volume (P-V) relation, we derive mode Grüneisen parameters from the data.

We report measurements of the Raman phonons in PbF_2 at room temperature, extending the previous measurements from 35 kbar up to 310 kbar. We verify the previously observed $\beta \rightarrow \alpha$ phase transition at about 4 kbar.[12] Our data also demonstrate the existence of a high-pressure phase of PbF_2 above 147 kbar, which is structurally similar to the α phase; we label this modification γ. Two candidate crystal structures for this γ phase are (1) a hexagonal structure observed recently in BaF_2 (Ref. 13) and (2) a monoclinic structure observed in $PbCl_2$,[14,15] both of which represent only small perturbations from the orthorhombic α phase structure. The hexagonal structure can be ruled out because the number of symmetry-allowed Raman-active modes is less than the number of observed modes. Conversely, the Raman data are consistent with the monoclinic structure. The large number of atoms in the unit cell as well as independent degrees of freedom make calculations for the monoclinic structure intractable. However, our first-principles calculations for the hexagonal structure show that it becomes stable relative to the orthorhombic structure for pressures greater than 164 kbar. Two important conclusions can be drawn from these calculations despite the fact that the hexagonal structure is ruled out experimentally; the first is that a structural instability in the α phase occurs in this pressure range; the second is that 164 kbar is an upper bound for the transition pressure, as a more energetically favorable structure, known to exist experimentally, would result in a lower calculated transition pressure.

In summary, our combined experimental and theoretical results establish important constraints to understanding the properties of PbF_2, which may then provide the basis for developing a number of technological applications. The remainder of this paper is organized as follows. We present a brief background discussion on PbF_2 in Sec. II. In Sec. III we describe the fundamental characteristics of the two experimentally observed low-pressure crystal structures as well as the high-pressure hexagonal structure observed in BaF_2. The results from our Raman measurements and theoretical analysis are presented in Secs. IV and V, respectively. Finally, a detailed discussion of our results is given in Sec. VI.

II. BACKGROUND

We briefly review some of the properties of PbF_2. Superionic conductors have anomalously high electrical conductivities, comparable to those of melts or liquid electrolytes. The superionic characteristics of β PbF_2 have been studied

extensively at low pressures.[5–7,16–18] At 1 bar, the system undergoes a second-order transition over a broad temperature range of 475–775 K, to a highly conductive superionic state.[19,20] A lattice disordering has been observed to occur in approximately the same temperature range.[19,20] The conductivity is given by[21]

$$\sigma(T)=\sigma_0\exp\left[-\frac{E_A}{k_BT}\right], \tag{1}$$

where σ, T, σ_0, E_A, and k_B are the conductivity, temperature, high-temperature conductivity limit, activation energy barrier, and Boltzmann's constant, respectively. In the superionic state the activation energy describing the electrical conductivity decreases from about 0.52 to 0.26 eV, ultimately leading to a conductivity at 800 K of approximately 2 Ω^{-1} cm^{-1}.[7,22] Recent theoretical investigations suggest that the fluorine-ion (F^-) sublattice becomes mobile as these ions ''melt'' within a rigid matrix of the lead-ion (Pb^{+2}) sublattice.[23] This disorder of the F^- ions (Frenkel defects) is manifested in the Raman spectra by a characteristic asymmetry in the line shape of the F_{2g} mode, as previously reported.[17,24] PbF_2 has one of the highest solid-phase superionic conductivities of any material known.

Interest in the optical properties of PbF_2 has been elevated by recent reports that the material has characteristics relevant to high-energy particle detector applications. In 1990, Anderson *et al.* reported that PbF_2 was a promising radiation-resistant Cherenkov radiator.[3] Subsequently, Baliakin *et al.* reported that the amorphous or highly deformed α phase of PbF_2 scintillated.[8] The β phase has not been stimulated to scintillate, as the high mobility of the F^- ions is believed to nonradiatively quench excitations. Recently, Anderson *et al.* tried unsuccessfully to reproduce the scintillation in PbF_2 using hydrostatic pressure.[25]

The properties of PbF_2 have been studied extensively as a function of pressure. The elastic behavior has been explored experimentally and theoretically to about 3 kbar.[26–28] Samara has measured ionic conductivities of both the β and α phases to about 4 kbar and concluded that Frenkel defects are the dominant source of ionic conductivity in both phases.[7] Long-wavelength dielectric measurements found evidence for a soft transverse optical phonon, which indicates that PbF_2 has a ferroelectric mode.[18] The dielectric constant has also been measured at optical frequencies and has been found to vary linearly with pressure.[12]

Schmidt and Vedam originally observed the α phase at pressures greater than 4.8 kbar and were able to recover the structure at 1 bar.[12] The phase boundary in P-T space has been studied by differential thermal analysis and by dielectric signatures.[18,29] Infrared- and Raman-active modes have been measured to 45 and 35 kbar, respectively.[10,30] The structure of the β phase permits only one Raman-active mode, F_{2g}. A much weaker peak has been reported previously and correlated with imperfections in the lattice.[17] A semiempirical identification of the Raman modes in the α phase has been proposed by Kessler *et al.*[10]

III. CRYSTAL STRUCTURES

The β phase of PbF_2 occurs in the cubic fluorite structure,[31] which is open and common to a number of ionic materials. The fluorite structure can be derived from the zinc-blende structure by placing an additional F atom in the tetrahedral interstitial site. The octahedral interstitial site remains empty in both structures. The packing fraction[21] provides a purely theoretical measure of the degree to which a given crystal structure is open or close packed, and depends only upon the local atomic geometry and is independent of the chemical identity of the constituents. While the packing fraction is not uniquely defined when there is more than one atom type, we will adopt the convention of equal-sized Pb and F spheres, which is sufficient for providing a qualitative indication of the degree of openness.[21] With this convention, the packing fraction of the fluorite structure is 0.51. We note that there is adequate space in this structure to place another sphere of the same size in the octahedral interstitial site, which results in a packing fraction of 0.68, equal to that of the bcc structure.

At room temperature and approximately 4 kbar, PbF_2 transforms from the cubic β to the orthorhombic α phase ($PbCl_2$-type structure) with a corresponding 8% decrease in the volume per atom. The structure of the α phase consists of a 12-atom basis made up of four equivalent Pb atoms and two sets of four equivalent F atoms, which we label F1 and F2. Each set of four atoms occupies the following sites (Wyckoff label $4c$), in lattice coordinates:[31]

$$(x,y,\tfrac{1}{4}),\qquad (\tfrac{1}{2}-x,\tfrac{1}{2}+y,\tfrac{1}{4}),$$
$$(1-x,1-y,\tfrac{3}{4}),\quad (\tfrac{1}{2}+x,\tfrac{1}{2}-y,\tfrac{3}{4}),$$

where x and y are internal structural parameters. This structure can be viewed as two alternating planes of atoms stacked along the c axis. Because the structure is orthorhombic, in addition to the six internal parameters (two for each four-atom set), there are three independent lattice constants, a, b, and c.

BaF_2 also exhibits a transition from the cubic fluorite structure to the $PbCl_2$-type orthorhombic structure at 35 kbar,[10,13] followed by another transformation to a hexagonal Ni_2In-type structure above 150 kbar.[13] As mentioned in Sec. I, we have carried out first-principles calculations for PbF_2 in this structure. It consists of a six-atom basis composed of two equivalent Pb atoms and two sets of two equivalent F atoms, which we again label F1 and F2. The atoms occupy the following sites, in lattice coordinates:[13]

$$\begin{array}{llll} \text{Pb} & (\frac{1}{3},\frac{2}{3},\frac{1}{4}) & (\frac{2}{3},\frac{1}{3},\frac{3}{4}) & 2c,\\ \text{F1} & (\frac{1}{3},\frac{2}{3},\frac{3}{4}) & (\frac{2}{3},\frac{1}{3},\frac{1}{4}) & 2d,\\ \text{F2} & (0,0,0) & (0,0,\frac{1}{2}) & 2a, \end{array}$$

where the Wyckoff site labels are indicated to the far right. The two independent structural parameters are the lattice constants a and c.

IV. RAMAN MEASUREMENTS

A. Experimental techniques

High pressures were generated with diamond anvil cell techniques.[32] We based our cells on Mao-Bell and Silvera-Wijngaarden designs.[33,34] Our anvils were fabricated from

0.28-carat, low-birefringence, brilliant-cut diamonds with 350 μm diameter flat culets. Rhenium gaskets were drilled with approximately 150 μm diameter holes. The ruby scale was used for pressure determinations.[35,36] Argon was chosen as the pressure medium because of its lack of interfering Raman modes as well as its quasihydrostatic characteristics.

Our PbF_2 samples were typically from 20 to 80 μm in diameter and from 5 to 20 μm thick and were obtained by fracturing chips from a single crystal minutes prior to loading the sample. Care was taken to select the specimens from the center of the original crystal to avoid surface contamination. Crystalline orientation of the samples was undetermined, but measured Raman intensities were found to vary little with incident laser polarization or sample. We conducted four separate experiments, each experiment involving the study of several individual PbF_2 samples within the chamber. Pressure variations across the sample at low pressures were not measurable and at the highest pressure were less than 5 kbar. Because our measurements were spatially resolved, our uncertainty in pressure was less than this number, approximately ± 2 kbar at the highest pressures.

PbF_2 samples were probed with the 514.5 or 488.0 nm lines of an Ar^+ laser at power levels of 150 mW or less. The laser beam was focused to about a 20 μm diameter spot on the sample to avoid heating effects. No measurable changes in the spectra were observed as a function of laser power. Raman signals were measured in a backscattering geometry. Data were collected using Spex Triplemate 1877 and Spex 1704 spectrometers with liquid-nitrogen-cooled Princeton Instruments charge-coupled device (CCD) detectors. Raman signals were collected for frequencies greater than 100 cm^{-1} and required about 3 min of integration time.

B. Experimental results

We initially pressurized some samples to about 1 kbar to permit the study of the $\beta \rightarrow \alpha$ transformation. Typical spectra characterizing the two phases are plotted in Fig. 1. We observed a dominant and a minor peak in the β phase, as previously reported.[17] The minor peak occurs at low frequencies and has been attributed to lattice imperfections.[17] The ruby-scale pressure measurements were accurate to about 1 kbar at these low pressures. We determined the $\beta \rightarrow \alpha$ transition to occur at about 4 kbar. We note that the frequency of the imperfection mode decreases rapidly with increasing pressure.

The $\beta \rightarrow \alpha$ phase transition splits the dominant β phase peak into four broad peaks (Fig. 1) that sharpen and further separate with increasing pressure. We explored the hysteresis of the α phase Raman modes in one experiment up to 77 kbar (Fig. 2). We were able to characterize the phonon modes up to 310 kbar, and we plot the peak frequencies in Fig. 3 for all pressures. Representative spectra are shown in Fig. 1.

Peak frequencies in Figs. 2 and 3 were derived using a least-squares line shape fitting analysis. The uncertainty in the peak frequencies as determined from this analysis is significantly less than the variations between different experiments. These latter variations may result from unaccounted pressure gradients and sample differences, as well as measurement uncertainties.

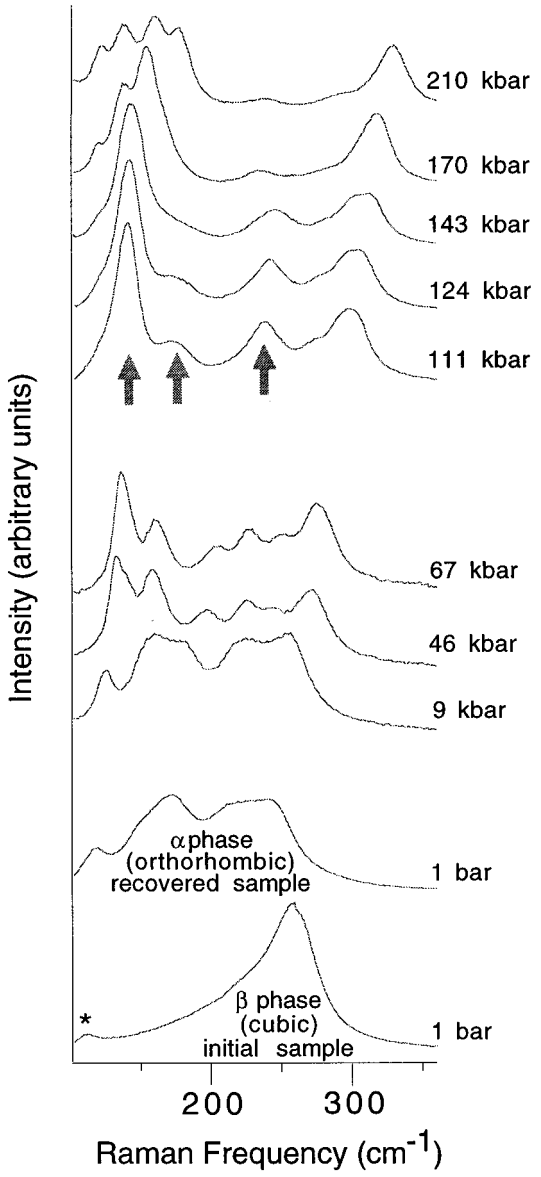

FIG. 1. Representative Raman phonon spectra at different pressures. The 1 bar spectra are from the two structures that are recoverable at ambient conditions. A weak peak in the β phase near 110 cm^{-1} (marked by a $\star$) indicates the presence of disorder. Above 4 kbar, the α phase structure is stabilized and is recoverable upon release of pressure. The initially broadbands in the α phase become progressively more distinct with increasing pressure. At about 147 kbar, changes in spectra indicate the $\alpha \rightarrow \gamma$ transition. The ~ 140 cm^{-1} A_{1g} peak splits into four distinct peaks. The ~ 170 cm^{-1} A_{1g} and ~ 245 cm^{-1} B_{2g} and A_{1g} peaks both become weaker as the transition approaches. These three modes are identified by the arrows.

V. FIRST-PRINCIPLES CALCULATIONS

A. Theoretical method

In addition to the Raman measurements, we have calculated the P-V EOS for α, β, and hexagonal PbF_2 using a first-principles, full-potential linear muffin-tin orbital (FP-LMTO) total-energy method,[37,38] which is based upon the local density approximation (LDA). We used a basis composed of 34 orbitals per atom. As is customary, we included

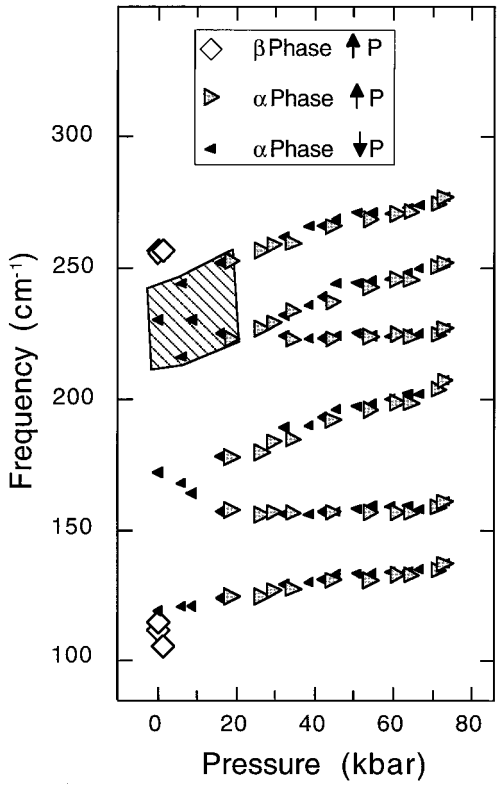

FIG. 2. Hysteresis of Raman phonon peak frequencies in α-PbF_2 is negligible. With increasing pressure (▶), the β phase transforms to the α phase at ~4 kbar. With decreasing pressure (◀), the α phase frequencies show no measurable hysteresis. However, the α phase persists to 1 bar. The shaded area indicates broadening of the bands.

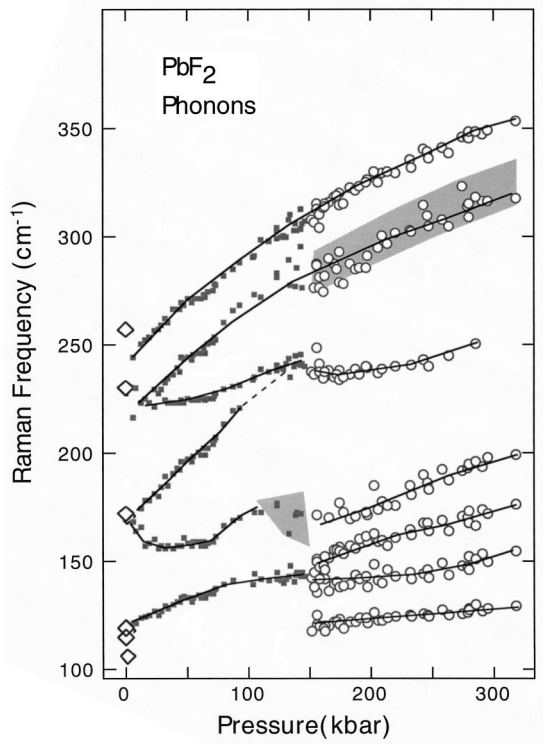

FIG. 3. Raman phonon frequencies in PbF_2 from 0 to 310 kbar for the β (◇), α (■), and γ (○) phases. The lines are guides to the eye. Shaded areas indicate broadened bands.

an empty atomic sphere at the octahedral interstitial site of the fluorite structure, solely for the purpose of improving the accuracy of the interpolation procedure used for evaluating interstitial integrals. We did not use any empty spheres for the orthorhombic or hexagonal structures.[39]

The calculations described here were scalar relativistic and based on the exchange-correlation potential of Hedin and Lundqvist.[40] We will present results from calculations which employed only the standard LDA, but most of the results reported here included the gradient corrections of Langreth, Mehl, and Hu (LMH).[41] We neglected spin-orbit interactions which is justified because the states derived from the Pb $6p$ orbitals are unoccupied. The Pb semicore $5p$ states were treated as full band states by carrying out a ''two-panel'' calculation. The Brillouin zone sums were carried out using 10 (2), 12 (2), and 36 (8) irreducible **k** points in the first (second) panel for the fluorite, orthorhombic, and hexagonal structures, respectively.

The six internal structural parameters, b/a, and c/a for the orthorhombic structure, as well as c/a for the hexagonal structure, were all determined by minimizing the total energy at fixed volume. The minimizations were performed with the aid of a numerical implementation of the analytical forces derived by Methfessel and van Schilfgaarde.[42] The calculated packing fractions reported here for the orthorhombic structure were obtained using an algorithm[43] which captures qualitative trends in the degree of openness.

B. Theoretical results

The total energies calculated at 14 different volumes for the β phase were fit using the Murnaghan form[44] in order to extract the cohesive energy, equilibrium volume, bulk modulus, and derivative of the bulk modulus. The calculated values correspond to $T=0$ K. The results obtained with and without gradient corrections are both compared to experiment in Table I. The calculated cohesive energies in Table I include spin-polarization contributions for the free atoms. In view of the significantly better agreement between experiment and the β-phase calculations carried out using gradient corrections, we have included these corrections in all of the calculations for the orthorhombic and hexagonal structures.

The structural parameters for the α phase were determined at ten different volumes. The values of these parameters as well as the lattice constant are plotted as a function of volume in Figs. 4–6. The experimental values at the observed equilibrium volume[45] are also shown as the open squares. The close agreement between these experimental values and the calculations confirms the accuracy of the calculational method despite the small packing fractions near the equilibrium volume (~0.5). From Fig. 7 we see that the packing fractions increase dramatically as the volume is reduced. The largest values of 0.64 are similar to the bcc close-packed value of 0.68.

We have employed the following procedure to obtain the pressure at each of the ten volumes shown in Figs. 4–6. We have used the cubic spline interpolations of the calculated structural parameters (see Figs. 5 and 6) to approximate the volume dependence of these parameters (the lattice constant a is determined from the volume and the values of b/a and c/a). For each of the ten original volumes, we then carried

TABLE I. Calculated cohesive energy per atom, E_{coh}, equilibrium volume per atom, V_0, bulk modulus B_0, and derivative of the bulk modulus, B_0' for the β and α phases of PbF_2 compared to experimental values where available. The results for the β phase were obtained both with (LDA+LMH) and without (LDA) gradient corrections. The calculated cohesive energies include spin-polarization contributions for the free atoms.

E_{coh} (eV/atom)	LDA	LDA+LMH	Experiment
α-PbF_2		3.896	
β-PbF_2	4.759	3.902	
V_0 (Å^3/atom)			
α-PbF_2		16.54	16.01[a]
β-PbF_2	16.62	17.54	17.47[b]
B_0 (Mbar)			
α-PbF_2		0.40	
β-PbF_2	0.85	0.71	0.62[c]
B_0'			
α-PbF_2		4.3	
β-PbF_2	4.8	4.8	

[a]Reference 45.
[b]Reference 47.
[c]Reference 48.

out a series of calculations over a small volume range centered at the original value, with the parameters obtained using the approximated volume dependence.

The pressures calculated in this way at the ten volumes were then fit using the Murnaghan EOS which relates the volume to pressure:[44]

$$\frac{V}{V_0}=\left[1+\frac{B_0'P}{B_0}\right]^{-1/B_0'}. \quad (2)$$

The resulting values of the fit parameters are listed in Table I along with those for the β phase. The pressure as a function of volume is plotted in Fig. 8 for both the β and α phases. Using these calculated EOS, we predict a $\beta\rightarrow\alpha$ transition pressure of 10 kbar at 0 K. However, the magnitude of the energy difference between the β and α phases (see Table I)

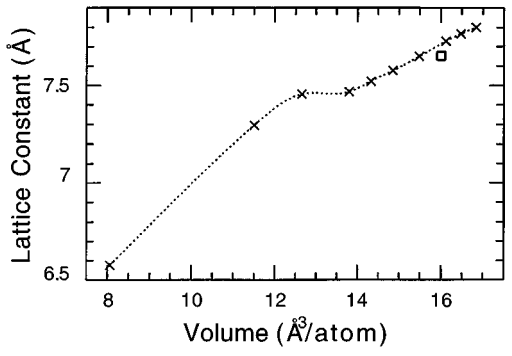

FIG. 4. The calculated lattice constants a for the α phase at ten different volumes (crosses). The dotted line corresponds to a cubic spline interpolation through the calculated values. The experimental value at the observed equilibrium volume (Ref. 45) is indicated by the open square.

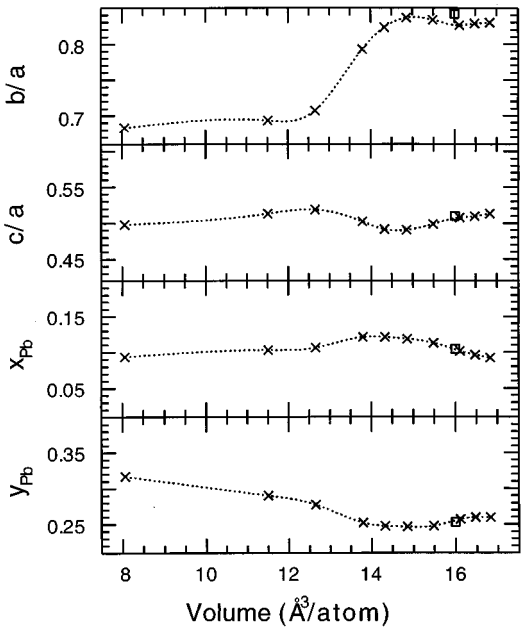

FIG. 5. The calculated axial ratios b/a and c/a as well as the two internal structural parameters for the Pb atoms in the α phase at ten different volumes (crosses). The dotted lines are cubic spline interpolations through the calculated values. The experimental values at the observed equilibrium volume (Ref. 45) are indicated by the open squares.

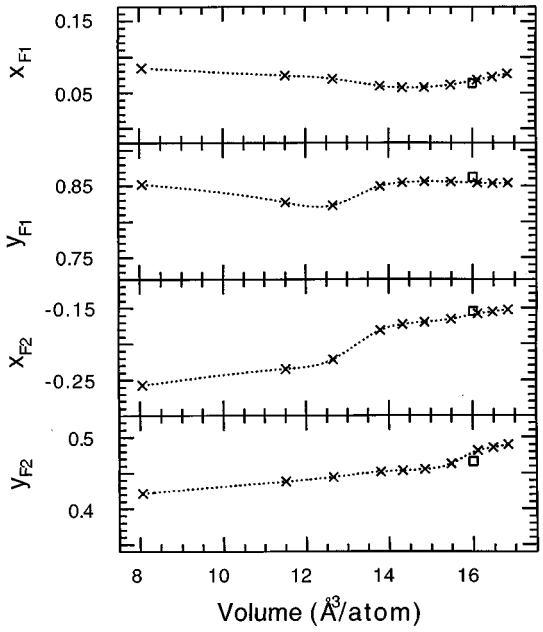

FIG. 6. Calculated internal structural parameters for the F1 and F2 atoms in the α phase at ten different volumes (crosses). The dotted lines are cubic spline interpolations through the calculated values. The experimental values at the observed equilibrium volume (Ref. 45) are indicated by the open squares.

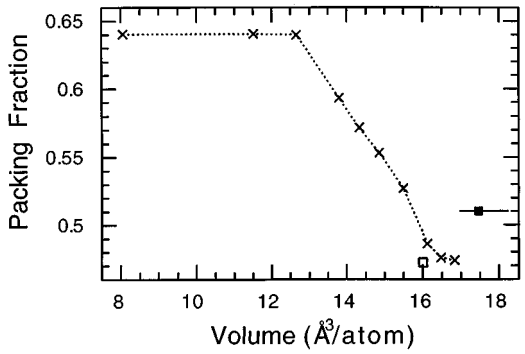

FIG. 7. Packing fractions (Ref. 43) as a function of volume for the β (solid line) and α (crosses) structures. The dotted line is a guide to the eye. The packing fractions for the observed structures are indicated by the solid and open squares for the β and α phases, respectively.

is smaller than the uncertainties inherent in the LDA method, and therefore, on the basis of the theory alone, we cannot state conclusively which phase is more stable. The Murnaghan form in Eq. (2) can also be used to calculate the bulk modulus, yielding a linear function of pressure:

$$B(P)=B_0+B_0'P. \tag{3}$$

In view of the transition at 147 kbar observed in this work, we have carried out a series of calculations for PbF_2 in the Ni_2In-type hexagonal structure, observed in BaF_2 above 150 kbar.[13] We have determined the values of c/a, ranging from 1.23 to 1.32, at eight different volumes, ranging from 8.1 to 14.3 Å^3/atom. We find that the packing fraction for this structure is approximately constant at a value of 0.61 over the volume range considered here, and therefore we have simply fit the total energy as a function of volume directly to the Murnaghan form.[44] Using this EOS and that of the α phase (Fig. 8), we obtain an orthorhombic→hexagonal transition pressure of 164 kbar at 0 K. As an aside, we find that the hexagonal structure is more stable than the orthorhombic structure for only a fixed range of volumes (pressures), with a reverse hexagonal→orthorhombic transition occurring at 424 kbar.

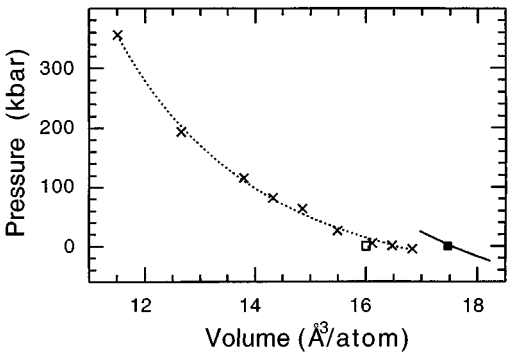

FIG. 8. P-V EOS for the β (solid line) and α (crosses) phases obtained using the procedures described in the text. The solid and dotted lines are fits to the calculated values using the Murnaghan form of Eq. (2). The corresponding fit parameters are listed in Table I. The equilibrium (zero-pressure) volumes for the observed structures are indicated by the solid and open squares for the β and α phases, respectively.

We briefly summarize our findings for the electronic structure. Consistent with the view of PbF_2 as an ionic solid, we find that the states derived from the F $2p$ orbitals are completely occupied (F^-), while the Pb $6p$-derived states are completely empty (Pb^{+2}). The states at the valence band maximum are predominantly antibonding combinations of F $2p$ and Pb $6s$ orbitals, while the states at the conduction band minimum are predominantly Pb $6p$ in character. These general characteristics of the electronic structure are essentially the same for both the α and β phases of PbF_2. The qualitative features of the electronic structure remain largely unchanged for all of the pressures studied here (from ambient conditions up to 2 Mbar for the α structure). In addition, the calculated energy gap decreases by only 20% over this same pressure range.[46]

VI. DISCUSSION AND CONCLUSIONS

The research described here has explored the dynamical and structural properties of PbF_2 over a wide pressure range. We now discuss our results.

Identification of the Raman modes for α-PbF_2 is summarized in Table II.[10] In previous work, Kessler *et al.*[10] measured PbF_2 spectra at 77 K and correlated the observed peaks to those of other divalent fluorides with the same structure. In contrast, our measurements were conducted at room temperature, and therefore the phonon spectra are comparatively broadened, such that some modes are no longer resolvable. Accordingly, only some of the peaks in our spectra have been classified.

We use the pressure dependence of the optical phonons to extract mode Grüneisen parameters. Qualitatively, most of the mode frequencies increase with rising pressure, behavior that is expected since the stronger interactions at higher pressures generally stiffen restoring forces. In Table II we use our calculated α phase P-V EOS (Fig. 8) to convert the mode frequency pressure dependence $d\omega_k/dP$ to the mode Grüneisen parameters, $-[\partial(\ln\omega_\kappa)/\partial(\ln V)]$, where ω_κ, P, and V are mode frequency, pressure, and volume, respectively. The mode Grüneisen parameters were found to vary with pressure and are well represented by linear functions (Table II). These parameters were only determined up to the limit of the stability regime of the α phase, namely, 147 kbar. Grüneisen parameters provide important constraints on interatomic potentials, since they depend qualitatively on the third derivative of the potentials.

We investigated the Raman modes in the β and α phases, with the specific intent of characterizing hysteresis effects. We increased the pressure of one sample from 1 to 77 kbar and slowly released the pressure to ambient conditions. Within our measurement error, no difference was observed in the spectra whether increasing or decreasing in pressure above 4 kbar (Fig. 2). Below 4 kbar, however, the α phase synthesized at high pressure is recovered at 1 bar, as noted previously.[5] Our calculations show that this result is due to the small energy difference between the α and β phases.

With increasing pressure, α-PbF_2 transforms to another, as yet undetermined, phase that we call the γ phase. The

TABLE II. Pressure dependence of Raman modes. Mode identification in α-PbF_2 at 77 K adapted from Kessler *et al.* (Ref. 10).

Symmetry	Frequency extrapolated to 1 bar at 77 K (Ref. 10)	Pressure dependence at 77 K (Ref. 10)	Pressure dependence (this work)	Mode Grüneisen parameter (this work)	
	ν (cm^{-1})	$\frac{d\omega_k}{dP}$ (cm^{-1} $kbar^{-1}$)	$\frac{d\omega_k}{dP}$ (cm^{-1} $kbar^{-1}$)	$\gamma_k=-\frac{\partial(\ln\omega_k)}{\partial(\ln V)}=a_k+b_kP$	
				a_k	b_k ($kbar^{-1}$)
A_{1g},B_{1g}	48	0.3			
B_{3g},B_{1g}					
A_{1g}	62	0.02			
B_{2g}	81	−0.08			
A_{1g}	124	0.26	0.15	0.503	3.93×10^{-3}
B_{1g}	127	0.47			
B_{3g}	151	0.19			
A_{1g}	172	−0.27	0.11	0.299	2.66×10^{-3}
B_{1g}	174	0.5	0.54	1.358	6.5×10^{-3}
B_{2g},A_{1g}	211	0.30	0.17	0.312	2.75×10^{-3}
B_{1g},B_{3g}	228	0.45	0.49	0.949	5.71×10^{-3}
B_{1g}	241	0.65			
A_{1g}	250	0.47	0.43	0.733	5.00×10^{-3}
B_{2g}	253	0.67			

transition is marked by the splitting of the 140 cm^{-1} A_{1g} mode, the disappearance of the 170 cm^{-1} A_{1g} mode, and the weakening of the ~245 cm^{-1} B_{2g} and A_{1g} modes (Fig. 1). Raman-active modes reflect the behavior of the $k=0$ region of the phonon bands and can identify the onset of a structural transition. The splitting of the 140 cm^{-1} A_{1g} mode does not appear to be purely a pressure narrowing of the modes, since the full width at half maximum (FWHM) of the peak shows a discontinuous change in slope with increasing pressure at about 147 kbar (Fig. 9). Hysteresis was briefly examined across the $\alpha\rightarrow\gamma$ transition. In one experiment, the onset of the transition was approximately 150 and 130 kbar with increasing and decreasing pressure, respectively. Within the pure α or γ phase, the phonon modes exhibited no measurable hysteresis.

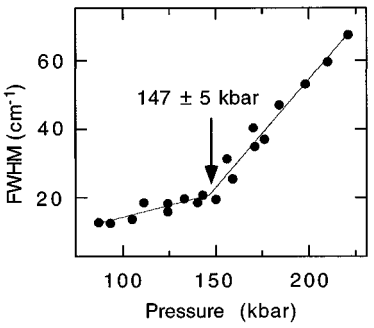

FIG. 9. FWHM of the 140 cm^{-1} A_{1g} mode is plotted for increasing pressure. A clear change in slope is observed near 147±5 kbar (uncertainty derived from a linear least-squares analysis). The discontinuous change in slope supports the identification of a phase transition.

At the $\alpha\rightarrow\gamma$ transition, the modes show no discontinuity in frequency and intensity. A reasonable interpretation of this behavior is that the new γ phase is a close derivative of the α phase. At the $\alpha\rightarrow\gamma$ transition, the 140 cm^{-1} A_{1g}mode splits into four separate peaks (Fig. 1). At 77 K in the α phase, three other Raman peaks are within close frequency vicinity of this A_{1g} mode,[10] whereas at room temperature, only two are resolved. Given that the FWHM increases starting at 147 kbar, we do not believe that the appearance of the four modes at room temperature is purely a pressure narrowing of the peaks. We cannot uniquely identify the structure of the γ phase based on current data, though the data suggests it is a small distortion of the orthorhombic structure. Below we discuss in detail the possible nature of the γ phase. The experimental phase diagram of PbF_2 is summarized in Fig. 10.

Since we believe that the γ phase is a modification of the orthorhombic structure, we examined the detailed atomic structure of the α-phase structure in the vicinity of 150 kbar in order to obtain insight into this new phase. From the calculated EOS (Fig. 8), we find that a pressure of 150 kbar corresponds to a volume of 13.2 $Å^3$/atom. We note that nearly all of the structural parameters are changing more rapidly in this volume range than in any other (Figs. 5 and 6). The largest change is an 18% decrease in the value of b/a. We also see that the lattice constant a remains nearly constant in this volume range, whereas it decreases monotonically with decreasing volume in all other ranges (Fig. 4). Last, we note that 13.2 $Å^3$/atom is close to the volume at which the packing fraction saturates at a value of 0.64 (Fig.

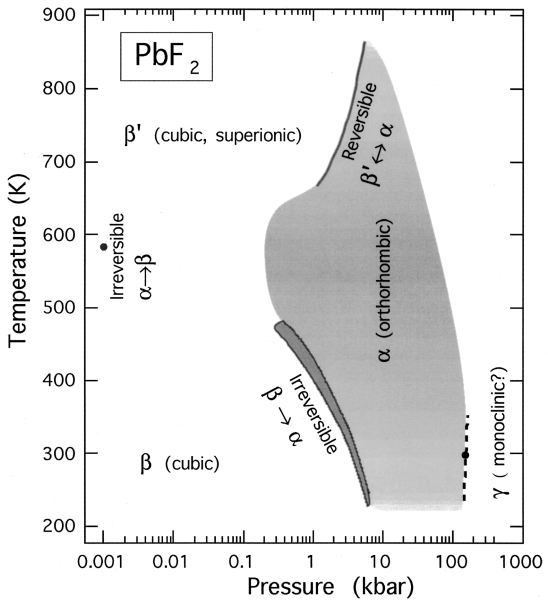

FIG. 10. Phase diagram of PbF_2. Summary of new data as well as previous results [see, e.g., Jamieson *et al.* (Ref. 26)]. At a few hundred degrees, the β phase transforms irreversibly to the α phase with increasing pressure. At ~700–800 K, the transition with rising pressure between $\beta' \leftrightarrow \alpha$ is reversible. β' is the cubic phase with the F^- ions disordered. A point is shown at 1 bar, $T \sim 580$ K, where the α phase (recovered from high pressures) transforms irreversibly to the β phase. The γ phase discovered here is shown at 150 kbar with a speculative dashed phase boundary.

7). The rapid changes in the structural parameters near 150 kbar support the possibility for a phase transition.

In Sec. V B we indicated that the calculated EOS for the α phase and a candidate γ phase hexagonal structure yielded a transition pressure of 164 kbar, which would appear to be in very close agreement with our experiments. However, the hexagonal structure is eliminated as a possibility because it has only two doubly degenerate symmetry-allowed Raman-active modes ($2E_{2g}$), while at least seven distinct modes are observed in the γ phase (Figs. 1 and 3). Nonetheless, the calculations are important because they demonstrate that there is a structural instability in the α phase in this pressure range. In addition, 164 kbar represents an upper bound for the transition pressure since there must be yet another even lower-energy structure which would yield a lower calculated transition pressure. In addition, it is likely that this alternate structure will have a calculated transition pressure close to 150 kbar given the rapid changes in the orthorhombic structural parameters near this pressure. Another candidate structure is that of the monoclinic phase observed recently in $PbCl_2$.[14,15] However, the large number of atoms in the unit cell and many independent degrees of freedom make calculations for this structure intractable. The number of observed Raman modes for the γ phase (Figs. 1 and 3) is at least consistent with the monoclinic structure. However, we might have expected to see a larger increase in the number of observed modes at the $\alpha \rightarrow \gamma$ transition, given that the monoclinic structure has nearly four times the number of distinct symmetry-allowed Raman-active modes compared to the orthorhombic structure. Conversely, since we believe that the γ phase is structurally similar to the α phase, the additional symmetry-allowed modes may simply be unresolved in our experiments.

Finally, we have analyzed the detailed atomic geometry of the orthorhombic structure for pressures above 150 kbar. We find that the local near-neighbor configurations become progressively more bcc-like with increasing pressure. In addition, the calculated electronic structure indicates that PbF_2 remains insulating until ultrahigh pressures, consistent with our observations up to 310 kbar. We believe that these results provide insight into the ultrahigh-pressure behavior of PbF_2, as the α and γ phases are experimentally similar.

VII. SUMMARY

In this work, our goal was to investigate the interatomic interactions present in PbF_2 at varying atomic separations. We used pressure to vary the atomic distances and the Raman-active phonons as the experimental probes. Our data demonstrate a phase transition in PbF_2 at about 147 kbar. We have also initiated an effort to calculate the properties of PbF_2 from first principles. The calculations support the existence of a transition in the 150 kbar pressure range, although the crystal structure of the phase is unknown. We present our calculations of the P-V EOS including a first-principles determination of the α phase internal structural parameters and their pressure dependence. Using the calculated α-phase EOS, we have determined Grüneisen parameters from the experimental data for several modes. These theoretical and experimental results should severely constrain physical models developed to predict the properties of PbF_2. The experimental and theoretical techniques used in this work are generally applicable to other divalent fluorides as well as more complex systems.

ACKNOWLEDGMENTS

We would like to acknowledge valuable discussions with V. Garcia-Baonza, A. K. McMahan, and M. P. Surh. This work was performed under the auspices of the U.S. Department of Energy by the Lawrence Livermore National Laboratory under Contract No. W-7405-ENG-48.

[1] W. Hayes, *Crystals With The Fluorite Structure* (Clarendon, Oxford, 1974).
[2] T. S. Aurora, D. O. Pederson, and S. M. Day, Phys. Rev. B **41**, 9647 (1990).
[3] D. F. Anderson *et al.*, Nucl. Instrum. Methods Phys. Res. A **290**, 385 (1990).
[4] J. Oberschmidt, Phys. Rev. B **24**, 3584 (1981).
[5] G. A. Samara, Ferroelectrics **17**, 357 (1977).
[6] M. Nizam and Y. Bouteiller, J. Mol. Struct. **206**, 99 (1990).
[7] G. A. Samara, J. Phys. Chem. Solids **40**, 509 (1979).
[8] S. N. Baliakin *et al.*, in *Heavy Scintillators for Scientific and Industrial Applications*, Proceedings of the ''Crystal 2000'' In-

ternational Workshop, edited by F. DeNotaristefani, P. Lecoq, and M. Schneegans (Editions Frontières, Paris, 1993), p. 587.
[9] C. Woody *et al.*, IEEE Trans. Nucl. Sci. **NS-40**, 546 (1993).
[10] J. R. Kessler, E. Monberg, and M. Nicol, J. Chem. Phys. **60**, 5057 (1974).
[11] D. L. Alov and S. I. Rybchenko, J. Phys., Condens. Matter. **7**, 1475 (1995).
[12] E. D. D. Schmidt and K. Vedam, J. Phys. Chem. Solids **27**, 1563 (1966).
[13] J. M. Leger, Phys. Rev. B **52**, 13 247 (1995).
[14] J. M. Leger, J. Haines, and A. Atouf, Phys. Rev. B **51**, 3902 (1995).
[15] J. M. Leger, J. Haines, and A. Atouf, J. Phys. Chem. Solids **57**, 7 (1996).
[16] I. Kosacki, M. Y. Wallach, and A. P. Litwinczuk, Solid State Commun. **53**, 373 (1985).
[17] I. Kosacki, A. P. Litvinchuk, and M. Y. Valakh, Acta Phys. Pol. A **77**, 299 (1990).
[18] G. A. Samara, Phys. Rev. B **13**, 4529 (1976).
[19] J. B. Boyce and B. A. Huberman, Phys. Rep. **51**, 189 (1979).
[20] A. Chadwick, Radiat. Eff. **74**, 17 (1984).
[21] N. W. Ashcroft and N. M. Mermin, *Solid State Physics* (Holt, Rinehart, and Winston, San Francisco, 1976).
[22] J. Kosacki, M. Walach, and A. P. Litwinczuk, Acta Phys. Pol. A **67**, 245 (1985).
[23] R. E. Benenson *et al.*, Phys. Rev. B **44**, 6663 (1991).
[24] W. Hayes *et al.*, J. Phys. C **10**, L111 (1977).
[25] D. F. Anderson *et al.*, Nucl. Instrum. Methods Phys. Res. A **342**, 473 (1994).
[26] J. C. Jamieson *et al.*, J. Geophys. Res. **91**, 4643 (1986).
[27] R. K. Singh and C. N. Rao, Pramana, J. Phys. **34**, 297 (1990).
[28] D. S. Rimai, M. H. Chao, and R. J. Sladek, Solid State Commun. **35**, 213 (1980).
[29] W. Klement and L. H. Cohen, J. Electrochem. Soc. **126**, 1403 (1979).
[30] J. R. Ferraro, H. Horan, and A. Quattrochi, J. Chem. Phys. **55**, 664 (1971).
[31] R. W. G. Wyckoff, *Crystal Structures* (Interscience, New York, 1963), Vol. 1.
[32] A. Jayaraman, Rev. Mod. Phys. **55**, 65 (1983).
[33] H. K. Mao and P. M. Bell, Science **191**, 851 (1976).
[34] I. F. Silvera and R. Wijngaarden, Rev. Sci. Instrum. **56**, 121 (1985).
[35] J. D. Barnett, S. Block, and G. J. Piermarini, Rev. Sci. Instrum. **44**, 1 (1973).
[36] H. K. Mao, J. Xu, and P. M. Bell, J. Geophys. Res. **91**, 4673 (1986).
[37] M. Methfessel, Phys. Rev. B **38**, 1537 (1988).
[38] M. Methfessel, C. O. Rodriguez, and O. K. Andersen, Phys. Rev. B **40**, 2009 (1989).
[39] We attempted to include empty spheres for the loosely packed orthorhombic structure, but the nature of the atomic geometry constrained them to have very small radii and thus a negligible effect on the overall packing fraction.
[40] L. Hedin and B. I. Lundqvist, J. Phys. C **4**, 2064 (1971).
[41] See, for example, P. Bagno, O. Jepsen, and O. Gunnarsson, Phys. Rev. B **40**, 1997 (1989), and references therein.
[42] M. Methfessel and M. van Schilfgaarde, Phys. Rev. B **48**, 4937 (1993).
[43] Two sets of sphere radii corresponding to the shortest nearest-neighbor distance (either Pb or F1 or Pb and F2, depending on the volume) were taken to be the same with the spheres exactly touching. The last set of radii (F2 or F1) were taken to be as large as possible, but still consistent with the criterion of touching spheres.
[44] F. D. Murnaghan, Proc. Natl. Acad. Sci. USA **30**, 244 (1944).
[45] P. Boldrini and B. O. Loopstra, Acta Crystallogr. **22**, 744 (1967).
[46] The LDA generally underestimates energy gaps, but the derivative of the gap as a function of pressure is typically more accurate, and therefore we expect that 20% is an upper bound.
[47] W. Pies and A. Weiss, *Numerical Data and Functional Relationships in Science and Technology*, New Series (Springer-Verlag, Berlin, 1973), Vol. 7a.
[48] A. G. Every and A. K. McCurdy, *Numerical Data and Functional Relationships in Science and Technology*, New Series (Springer-Verlag, Berlin, 1992), Vol. 29.